

# Understanding the negative vacancy in silicon without configuration interaction theory

U. Gerstmann, E. Rauls, H. Overhof,\* and Th. Frauenheim

*AG Theoretical Physics, Physics Department, University of Paderborn, D33095 Paderborn, Germany*

(Received 13 July 2001; revised manuscripts received 19 September 2001; published 18 April 2002)

We have calculated the electronic structure of the lattice vacancy in silicon in the negative charge state  $V^-$  using the self-consistent charge density-functional theory based tight-binding scheme for the computation of large supercells containing up to 512 atoms in combination with the linear muffin-tin orbitals method in the atomic-spheres approximation. Many-body effects are treated in the local spin density approximation of the density functional theory (LSDA-DFT). We find the ground state of the  $V^-$  to be the low-spin  ${}^2B_1$  state of the group  $C_{2v}$ , which is lower in energy by 0.09 eV than the  ${}^4A_2$  high-spin state of the group  $T_d$ . We have also calculated the hyperfine interactions with 18 shells containing 46  ${}^{29}\text{Si}$  ligand atoms. We find the largest HF interactions in the  $(\bar{1}\bar{1}0)$  plane in agreement with experimental data. The HF interactions with nuclei in the  $(110)$  plane, which are about two orders of magnitude smaller than those with nuclei in the  $(\bar{1}\bar{1}0)$  plane, also agree with the experimental data. We conclude that the LSDA-DFT describes the magnetization density of the  $V^-$  well. It is therefore not necessary to include configuration interactions as has been proposed by M. Lannoo [Phys. Rev. B **28**, 2403 (1983)].

DOI: 10.1103/PhysRevB.65.195201

PACS number(s): 76.30.Da, 71.15.Mb, 71.55.Cn, 71.55.-i

## I. INTRODUCTION

The lattice vacancy in silicon is a defect of fundamental interest, because it presents the place into which the substitutional defect atoms have to be inserted. Conceptually, it might be considered to be the most simple deep defect, as it consists of one missing lattice atom in the diamond lattice of an elemental semiconductor. However, in the first review<sup>1</sup> on electron paramagnetic resonance (EPR) spectra of the vacancy it was noted that the electronic structure of this deep defect is quite complex with different symmetry-lowering Jahn-Teller distortions for the different charge states of the vacancy. But the experimentally observed distortions, a  $D_{2d}$  distortion of  $V_{\text{Si}}^+$  and a  $C_{2v}$  distortion of  $V_{\text{Si}}^-$  could be successfully explained in a simple linear combination of atomic orbitals (LCAO) one-electron picture.<sup>1,2</sup>

In contrast, the calculation of the electronic structure of the vacancy using *ab initio* methods proved to be a major challenge to the theorists. The first calculations successfully explained the negative- $U$  property of the positive charge state of the vacancy<sup>3,4</sup> which was proven experimentally,<sup>5</sup> and the formation energies reported by different groups were quite comparable. However, the calculation of the lattice relaxation turned out to be quite cumbersome (see, e.g. Refs. 6–9): the energy surface is found to be extremely flat such that the calculated position of the total energy minimum in the coordination space and even the calculated symmetry of the relaxed defect depends on computational details such as supercell size and  $k$ -point sampling. In fact, for the negative charge state of the vacancy, the apparently most accurate and sophisticated calculation<sup>7</sup> obtains a relaxation into a state of  $D_{3d}$  symmetry, in contrast to the  $C_{2v}$  symmetry which was predicted by the LCAO model calculation in agreement with the experiment.<sup>1</sup>

Practically all calculations of lattice relaxations around the isolated vacancy in silicon have been performed using the local density approximation to the density-functional theory (LDA-DFT) ignoring spin polarization effects, most

of them dealing with the spinless neutral vacancy  $V^0$ . For this charge state experimental data are rare. For the vacancy in the paramagnetic  $V^-$  charge state detailed experimental information is available from EPR (Ref. 1) and electron nuclear double resonance (ENDOR) experiments.<sup>10</sup> Yet a single calculation of the hyperfine (HF) interactions with the ligand nuclei for  $V^-$  (Ref. 11) has been presented to date. This calculation, also based on the LDA-DFT ignoring spin polarization effects, simulates the magnetization density by the particle density distribution of the singly occupied single-particle gap state. Since this state transforms according to the  $b_1$  irreducible representation of the point group  $C_{2v}$ , it has a  $(110)$  nodal plane, while the particle density is concentrated in the  $(\bar{1}\bar{1}0)$  plane. Therefore, for all nuclei within the  $(110)$  plane containing the vacancy [including the nuclei on the cubic  $(001)$  axis] the isotropic HF interactions in a LDA-DFT calculation must vanish.<sup>11</sup>

In contrast, experimental ENDOR data<sup>10</sup> exhibit small but nonzero contact HF interactions with several shells of nuclei within the  $(110)$  plane. Lannoo<sup>12</sup> has shown that the order of magnitude of these interactions can be accounted for in the LCAO picture if excited states are included in a configuration interaction (CI) scheme. This raises the question whether it is necessary to use the full CI apparatus in order to explain the small contact interactions with nuclei on the  $(110)$  plane. The CI scheme has the disadvantage that for systems such as the vacancy in a solid the large number of competing configurations prohibits a quantitative evaluation.

The CI explanation for the nonzero HF contact interactions was challenged by Sprenger *et al.*<sup>10</sup> who emphasize exchange polarization effects that can lead to a similar result. In the local spin density approximation of the density-functional theory (LSDA-DFT), the spin density is represented by that of the Kohn-Sham orbitals. A paramagnetic state with spin 1/2 can be obtained by the occupation of one gap state with spin up, leaving the spin-down state of this orbital unoccupied. If all other Kohn-Sham orbitals are either unoccupied or occupied both for spin-up and spin-down, the

magnetization density reflects the symmetry of the spin-up orbital. But in a self-consistent calculation which includes the spin polarization via the exchange interaction, the spin polarization of this spin-up orbital is in part transferred to the other orbitals. Therefore the resulting magnetization density does not necessary vanish on the nodal plane of the spin-up orbital. It is an interesting problem to investigate, whether the magnetization density transferred in the LSDA-DFT scheme is sufficient to explain the order of magnitude of the HF contact interactions observed experimentally<sup>10</sup> or whether the full apparatus of CI is required.

We investigate this question in the present paper. We start in the next section calculating the relaxed atomic geometry for the  $V^-$  state of the vacancy using supercells. With the atomic coordinates thus obtained we calculate the hyperfine interactions in a LSDA-DFT Green's function approach. We show that while the larger interactions are found for nuclei in the  $(1\bar{1}0)$  plane, much smaller interactions are found for nuclei in the  $(110)$  plane as observed experimentally. The fair agreement of calculated HF interactions with experimental ENDOR data<sup>10</sup> leads us to the conclusion, that there is no need to include CI into the calculation of the electronic state of  $V^-$ .

## II. TOTAL ENERGY CALCULATION OF THE RELAXED GEOMETRY

In our approach we perform a LSDA calculation including spin polarizations using the relaxed coordinates obtained from a separate spin-unpolarized calculation. This can be justified as lattice relaxations are governed by the charge density. From our spin-polarized calculations we find the charge densities of all localized states to be rather insensitive to the spin state. We thus are confident that the lattice relaxations calculated within the LDA are fairly accurate. Of course, for the relaxation energies we have to consider the spin alignment energies as well. This is essential in order to decide whether a high-spin or a low-spin ground state is predicted for the  $V^-$  charge state. In a first step we have calculated the atomic geometry of the  $V^-$  defect using the self-consistent charge density-functional theory based tight-binding scheme (SCC-DFTB).<sup>13</sup> The tight-binding parameters have been chosen to reproduce the experimental lattice constant and the bulk modulus of crystalline silicon, i.e., to optimize the structural properties. Since in Ref. 7 the resulting defect symmetry was strongly depending on the size of the supercell and also on the  $k$ -point sampling, we have made use of different supercells.

These included sc supercells containing 64, 216, and 512 atoms and fcc cells with 128 and 250 atoms, respectively, using  $\Gamma$ -point sampling. For the 216 atom supercell we have also used the  $2 \times 2 \times 2$   $k$ -point Monkhorst-Pack sampling scheme.<sup>14</sup> The positions of all atoms have been relaxed in a conjugate-gradient formalism. Since the energy contour in the coordinate space for the vacancy in all charge states is known to be extremely flat<sup>7-9</sup> we started the relaxation with different point group symmetries ( $T_d, D_{2d}, C_{2v}, C_{3v}$ , and  $D_{3d}$ ), maintaining the symmetry constraint during each relaxation run. We have also relaxed the atomic positions with-

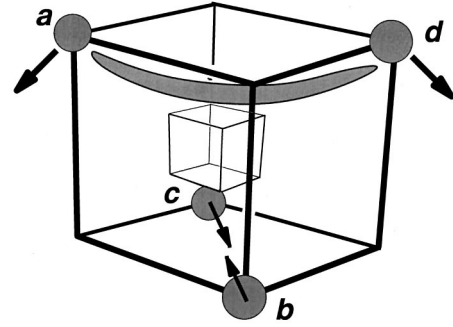


FIG. 1. Structural model of the  $V^-$  state of the vacancy (center). The directions of the  $C_{2v}$  distortion are indicated by the arrows.

out symmetry constraints. In this calculation we found the same minimum that was found for a relaxation with the appropriate symmetry constraint.

In contrast to the results of plane-wave expansions reported in Refs. 7,8 we do not observe qualitative differences between the results obtained from the 64 atom supercells and those obtained from larger cells and with different  $k$ -point samplings. Thus in our case the use of a tight-binding scheme seems to suppress the critical convergence problems observed for the first-principles supercell calculations.<sup>7,8</sup> For the  $V^-$  the apparently best first-principles calculation<sup>7</sup> predicts a ground state with a  $D_{3d}$  Jahn-Teller distortion. But as the distortion energies for the symmetry lowering distortions are extremely small (see below), the fact that our calculations gives a ground state with  $C_{2v}$  symmetry as observed experimentally may be just fortunate, although we would prefer to attribute this fact to the use of tight-binding parameters that are optimized with respect to the structural properties of silicon.

For the  $V^{2+}$  charge state the minimum of the total energy was found for a breathing relaxation that conserved the  $T_d$  symmetry. The four nearest neighbors of the vacancy move inwards by 19% corresponding to an energy gain of 1.1 eV. For the positive (neutral) charge states a tetragonal Jahn-Teller distortion leads to an additional gain of 0.12 eV (0.29 eV) and lowers the defect symmetry to  $D_{2d}$ . For the negative charge state the 15% inwards relaxation of the nearest neighbors contributed 1.25 eV.

When relaxing the four nearest neighbors only, the two neighbors  $a$  and  $d$  in the  $(1\bar{1}0)$  plane (see Fig. 1) move towards each other to a distance of 3.26 Å, while the distance between the neighbors  $b$  and  $c$  decreases slightly less to 3.34 Å. A similar relaxation was observed by Sugino and Oshiyama<sup>11</sup> in their 64 atom supercell. However, when relaxing the next nearest neighbors as well, the orthorhombic distortion is reversed, with an  $a$ - $d$  distance of 3.13 Å, significantly larger than the  $b$ - $c$  separation of 2.98 Å. The resulting relaxed coordinates (taken from the 216 atom supercell calculation with  $\Gamma$ -point sampling) for  $V^-$  are listed in Table I.

The relaxations are largest for the zigzag chain in the  $Mbc$  plane, although the spin density is very small in this plane. The relaxations in the  $Mad$  zigzag chain, however, are only slightly smaller. Note that the additional tetragonal

TABLE I. Relaxed coordinates of the ligands for  $V^-$  in silicon in units of  $a_0/4$  with  $a_0=5.428 \text{ \AA}$ .

Shell type	Unrelaxed			Relaxed		
<i>Mad</i> plane	1.00	1.00	1.00	0.80	0.80	0.88
	2.00	2.00	0.00	1.92	1.92	0.05
	3.00	3.00	1.00	2.96	2.96	0.99
<i>Mbc</i> plane	1.00	-1.00	-1.00	0.73	-0.73	-0.94
	2.00	-2.00	0.00	1.86	-1.86	-0.02
	3.00	-3.00	-1.00	2.92	-2.92	-0.98
General ( <i>G</i> type)	0.00	2.00	2.00	0.03	1.94	1.98
	0.00	-2.00	-2.00	-0.01	-1.95	-1.98

and a final orthorhombic distortion accounted for 0.17 and 0.03 eV, respectively, to the total relaxation energy, much less than the 1.25 eV relaxation energy contributed by the breathing distortion.

Qualitatively these relaxations can be understood from the

particle density distribution. We show in Fig. 2 contour plots of the particle density for the  $a_1''$  and  $b_1$  gap states in two (001) planes, one passing through the  $a$  and  $d$  nearest neighbor ligands, and the other passing through the  $b$  and  $c$  ligands (see Fig. 1). We also show the contour plots in a the (010) plane that contains ligands  $b$  and  $d$ . For the  $a_1''$  state we find a bondlike particle density bridging both the  $a-d$  and the  $b-c$  distance. In the (010) plane the density shows a minimum between  $b$  and  $d$  demonstrating that the  $a_1''$  state originates from a  $t_2$  state. While the density arising from the  $a_1''$  state would be compatible with a  $D_{2d}$  defect symmetry, the density of the  $b_1$  state (occupied for spin-up only) clearly shows the defect to have the lower  $C_{2v}$  symmetry. There is an antibonding-like density bridging ( $a-d$ ), but no similar structure for ( $b-c$ ). For ligand  $b$ , the nodal plane of the  $B_1$  spin density is clearly observed. The essential antibonding character of the  $b_1$  bridge between atoms ( $a-d$ ) explains why for these atoms the distance exceeds the ( $b-c$ ) distance.

In a single-particle picture, the  $C_{2v}$  relaxation of  $V^-$  is easily explained if we consider the gap states shown in Fig.

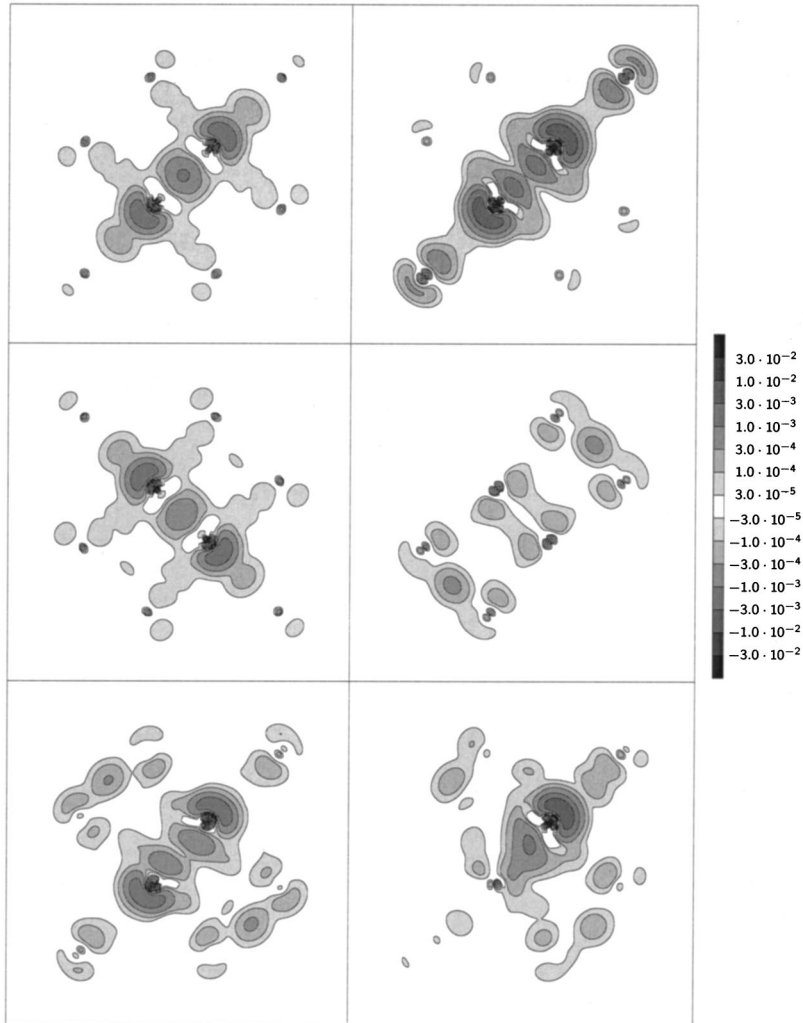


FIG. 2. Contour plot of the spin density for the  $V^-$  vacancy. Shown are the densities for the  $a_1''$  state (left column) and for the  $b_1$  gap states (right column). The densities are plotted in the (001) plane that passes through the ligands  $a$  and  $d$  (top) and through the ligands  $b$  and  $c$  (center). For comparison we show in the bottom line the contours in the (010) plane that contains the  $b$  and  $d$  ligands.

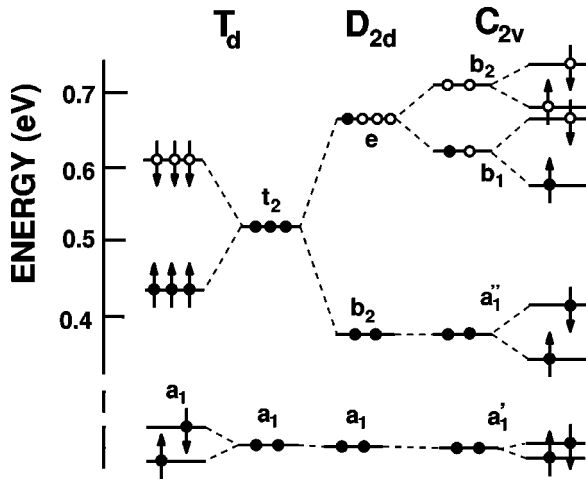


FIG. 3. Single particle states of the  $V^-$  relaxed with  $T_d$ ,  $D_{2d}$ , and  $C_{2v}$  Jahn-Teller distortion. For the  $T_d$  and  $C_{2v}$  distortion the respective spin splittings are also shown.

3. The (including spin degeneracy) twofold degenerate  $a_1$  state of the vacancy in  $T_d$  symmetry is a resonance just below the top of the valence band, whereas the  $t_2$  state is sixfold degenerate if we ignore the spin splitting. A tetragonal distortion splits the  $t_2$  state into a twofold degenerate  $b_2$  and a fourfold degenerate  $e$  state. For  $V^-$ , the twofold occupied  $b_2$  state is 0.25 eV below the  $e$  state, which is singly occupied. Since this state has a twofold orbital degeneracy, a further orthorhombic Jahn-Teller distortion sets in, splitting the  $e$  state into a  $b_1$  and a  $b_2$  state of the group  $C_{2v}$ . From these calculations that do not include spin polarization we would predict a  ${}^2B_1$  ground state for the relaxed state of  $V^-$ . Note, however, that there is the alternative  ${}^4A_2$  high-spin ground state for  $V^-$  in  $T_d$ , an orbital singlet state that is not subject to symmetry-lowering Jahn-Teller distortions.

In order to discriminate between these two alternatives, we have calculated the spin polarization energies using the linear muffin-tin orbitals method in the atomic-spheres approximation (LMTO-ASA).<sup>15</sup> For the exchange-correlation potential we have used the LSDA results of Ceperley and Alder<sup>16</sup> in the Perdew-Zunger parametrization scheme,<sup>17</sup> including the (small) spin polarization of the core states. Inserting the relaxed coordinates obtained from the SCC-DFTB calculation, we obtain the contribution from the spin alignment to the total energy. Adding that to the relaxation energy obtained from the SCC-DFTB calculation we find that the energy of the high-spin  ${}^4A_2$  state of the relaxed  $V^-$  in  $T_d$  symmetry is by 0.09 eV larger than that of the  ${}^2B_1$  state in  $C_{2v}$  symmetry, in agreement with the ground state found experimentally.<sup>1</sup> This should be contrasted to the same charge state of the  $V_{Si}^-$  in 3C-SiC (Ref. 20) and of the  $V_C^-$  in diamond,<sup>21</sup> which both have the  ${}^4A_2$  high-spin ground state.

For a tetrahedrally relaxed  $V^-$  in silicon, the total energy gain obtained by spin alignment is only 0.11 eV, smaller by a factor of 3 (5) if compared with the respective value for the  $V_{Si}^-$  in SiC (for  $V_C^-$  in diamond). For these latter defects, a breathing relaxation that conserves the  $T_d$  symmetry is obtained<sup>18,19</sup> already within the LDA ignoring spin polarization. This is explained by the fact that the C dangling bonds

are much more localized than the Si dangling bonds and therefore, do not form the bridges between the ( $a-d$ ) and ( $b-c$ ) neighbors. Therefore  $V^-$  in Si has a  $C_{2v}$  low-spin state while the other vacancies in the negative charge state are in a high-spin state of  $T_d$  symmetry as has been shown experimentally.<sup>20,21</sup>

### III. HYPERFINE INTERACTIONS

For the hyperfine interactions with the ligands of  $V^-$ , the convergence in the self-consistent cycles was surprisingly slow and sensitive to the lattice relaxation. We have calculated the contact HF interactions neglecting spin polarization (as in Sugino *et al.*<sup>11</sup>) and compare the results with those of a calculation that includes the spin polarization. For the HF interactions with the  $Mad$  nuclei in the  $(1\bar{1}0)$  plane we find only minor changes. But of course, for the nuclei in the  $(110)$  plane (denoted by  $Mbc$  and by T, respectively) the contact HF interactions resulting from a calculation without spin polarization are zero by symmetry, but attain values up to 2 MHz, if the spin polarization is included via the LSDA-DFT.

Results of the calculation including the spin polarization are listed in Tables II and III for a calculation with unrelaxed lattice positions, however assuming a  ${}^2B_2$  ground state of the defect with a  $C_{2v}$  symmetry and for a calculation with the fully relaxed coordinates. These are compared with experimental ENDOR data.<sup>10</sup> Note that for the experimental data the absolute signs of the HF interactions have not been determined, taking positive values for all contact interactions. In Table II, the calculated contact interactions for the  $Mad$  nuclei are negative, corresponding to a positive spin density (the nuclear gyromagnetic factor for  ${}^{29}Si$  is negative). For the  $Mbc$  nuclei (except for  $Mbc5$ ) we obtain positive HF contact interactions corresponding to negative magnetization densities.

For the HF interactions with the  $Mad$  nuclei we confirm the assignment given by Sprenger *et al.*<sup>10</sup> and by Sugino *et al.*<sup>11</sup> The magnetization density is concentrated on the  $\langle 110 \rangle$  zig-zag bond chain and decays *on this chain* monotonically with the distance from the vacancy center. Such a behavior was predicted for the defect-induced charge of a tetrahedral defect by Kane<sup>22</sup> and is assumed to be valid in Ref. 10. We can confirm this assumption for the first three members of the bond chain for which we have calculated data. For the surprisingly small values of the HF interactions with the  $Mad$  nucleus at  $(1,1,3)$  no reliable identification with any of the many candidates in<sup>10</sup> is possible, although  $Mad10$  or  $Mad11$  could be possible assignments. Note that the agreement between experimental data and those calculated for the relaxed structure are much better (in particular for the anisotropic HF interactions with the nuclei  $Mad2$  and  $Mad3$ ) than for the theoretical results for  $V^-$  in the unrelaxed structure.

In contrast to the assumptions in Ref. 10 our calculated HF interactions with  $Mbc$  and  $G$  ligand nuclei do not decay monotonically. For the HF interactions with the nuclei  $Mbc1$  and  $Mbc5$  listed in Table II our identification with the experimental values coincides with the interpretation given by Sprenger *et al.*<sup>10</sup> The HF interaction with the  $Mbc5$

TABLE II. Ligand hyperfine parameters for the  $V^-$  in silicon. The HF interactions calculated for an unrelaxed  $V^-$  with a  $C_{2v}$  symmetry constraint and for the  $V^-$  with the relaxed coordinates from the SCC-DFTB calculation are compared with the experimental ENDOR data of Sprenger *et al.* (Ref. 10) for which the sign of the contact interactions was set to be positive.

Shell	Unrelaxed			Relaxed			Exp			
	$a$	$b$	$b'$	$a$	$b$	$b'$	$a$	$b$	$b'$	
<i>Mad1</i>	(1,1,1)	-230.4	-26.8	-0.1	-242.0	-22.9	-0.59	355.8456	22.3034	1.2629
<i>Mad2</i>	(2,2,0)	-21.0	-3.5	-0.37	-35.1	-7.4	-0.08	50.2032	5.4894	0.6627
<i>Mad3</i>	(3,3,1)	-26.4	-0.10	-0.04	-14.6	-3.17	-0.14	30.5211	3.6690	0.2911
<i>Mad</i>	(1,1, $\bar{3}$ )	0.12	-0.08	-0.05	-0.73	-0.26	-0.09			
<i>Mbc1</i>	(1, $\bar{1}$ ,3)	2.24	0.08	0.08	1.81	0.14	0.10	2.1058	0.1763	0.0969
<i>Mbc2</i>	(2, $\bar{2}$ ,0)	1.08	0.09	0.04	0.94	0.12	0.04	1.9976	0.2043	0.1757
<i>Mbc3</i>	(2, $\bar{2}$ ,4)	1.02	0.04	0.03	0.82	0.05	0.03	0.8305	0.0674	0.0358
<i>Mbc4</i>	( $\bar{2}$ , $\bar{2}$ ,4)	0.17	-0.002	0.003	0.25	-0.03	0.01	0.2096	-0.0319	0.0078
<i>Mbc5</i>	(1, $\bar{1}$ , $\bar{1}$ )	2.94	-0.28	0.20	-0.05	0.61	0.28	0.2038	0.6805	0.0744
<i>Mbc?</i>	(3,3, $\bar{1}$ )	0.21	-0.03	-0.01	0.02	-0.04	0.02			
<i>T1</i>	(0,0,4)	0.37	0.07	0.04	0.44	0.06	0.05	0.6662	-0.0741	-0.0323
<i>T2</i>	(0,0, $\bar{4}$ )	0.14	-0.03	-0.03	0.17	-0.12	0.03	0.2827	0.0327	0.0006

is exceptional, because the modulus of the dipolar interaction exceeds that of the contact interaction. Here the HF interactions calculated for the unrelaxed lattice show no similarity with the experimental data. In particular the large anisotropic HF interaction is not obtained unless we take into account lattice relaxations. The order of magnitude of the contact interaction with the nuclei on the nodal plane of the  $b_1$  single particle states is already correct if we consider the  $C_{2v}$  symmetry of the defect.

The identification proposed in Table II for the nuclei *Mbc2* and *Mbc3*, although somewhat tentative, can account for all *Mbc* ligands found experimentally. In addition we have a further *Mbc* ligand (3,3, $\bar{1}$ ) for which there is no experimental counterpart in Ref. 10. The small calculated HF values qualify the interaction with this nucleus to be hidden in the distant ENDOR line. For the *T* nuclei our identification agrees with that of Sprenger *et al.*<sup>10</sup> It should be noted that the absolute differences between calculated and experimental HF interactions with nuclei in the *Mbc* plane (that includes the two *T* nuclei) is small. The relative deviations are not small, but since the calculated values sensitively depend on

TABLE III. Ligand HF interactions calculated for  $V^-$  with the relaxed coordinates from the SCC-DFTB calculation for the nuclei that are neither in the *Mad* nor in the *Mbc* planes. The assignment of the calculated HF interactions to experimental data reported by 10 is very tentative.

Shell	$a$	$b$	$b'$	Assignment
(0,2,2)	0.51	-1.78	0.03	
(0, $\bar{2}$ , $\bar{2}$ )	-5.59	-1.96	0.10	<i>G2</i> ?
(3, $\bar{1}$ ,1)	0.32	0.09	0.02	
(3,1, $\bar{1}$ )	2.27	0.51	0.14	<i>G6</i> ?
(1,3,3)	-4.48	-1.10	0.10	<i>G3</i> ?
(1,3, $\bar{3}$ )	0.34	-0.19	0.06	

the details of the lattice relaxation, we must not expect the resulting magnetization densities to be very accurate.

For the interactions with the *G* nuclei that are neither on a *Mad* plane nor on a *Mbc* plane we find rather small values as is observed experimentally. Our identification with experimentally determined HF interactions is very tentative. Note that the assignment given by Sprenger *et al.*<sup>10</sup> for some of the *G* nuclei, which is also not secure, contains no nucleus that can be found in our perturbed region. On the other hand, we ascribe the two HF interactions *G2* and *G6* to the same lattice positions as Sugino and Oshiyama,<sup>11</sup> but do not agree with respect to their assignment regarding the other *G* nuclei.

The nonzero magnetization density in the (110) plane containing the *Mbc* nuclei is illustrated by the contour plots in Fig. 4. The large magnetization density in the (110) plane containing the *Mad* ligands is due to the  $b_1$  spin-up gap state, which has a node in the (110) plane. However, in the total magnetization density shown in Fig. 4 this nodal plane is at best hinted. The spin polarization of the  $b_1$  gap state gives rise to a small spin polarization of the other vacancy-induced states. For the  $a_1''$  gap state (occupied both with spin-up and spin-down) the induced magnetization density is negative and closely resembles the (positive) particle density both in the (110) and the (110) plane, whereas for the  $a_1'$  resonance the induced magnetization is positive in both planes. In summary, the total magnetization density in the (110) plane is positive in rather large regions between the nuclear positions, however with very small negative values at most of the *Mbc* nuclei.

A nonzero magnetization density of the gap states in the (110) plane could in principle be explained alternatively assuming the term order of the the  $a_1''$  and  $b_1$  single particle states to be reversed, leaving the  $a_1''$  singly occupied with a  $b_1$  state that is occupied by two electrons. This explanation has been discussed by Sprenger *et al.*<sup>10</sup> and by Lannoo<sup>12</sup> as being quite unlikely due to energetic reasons. We find that it

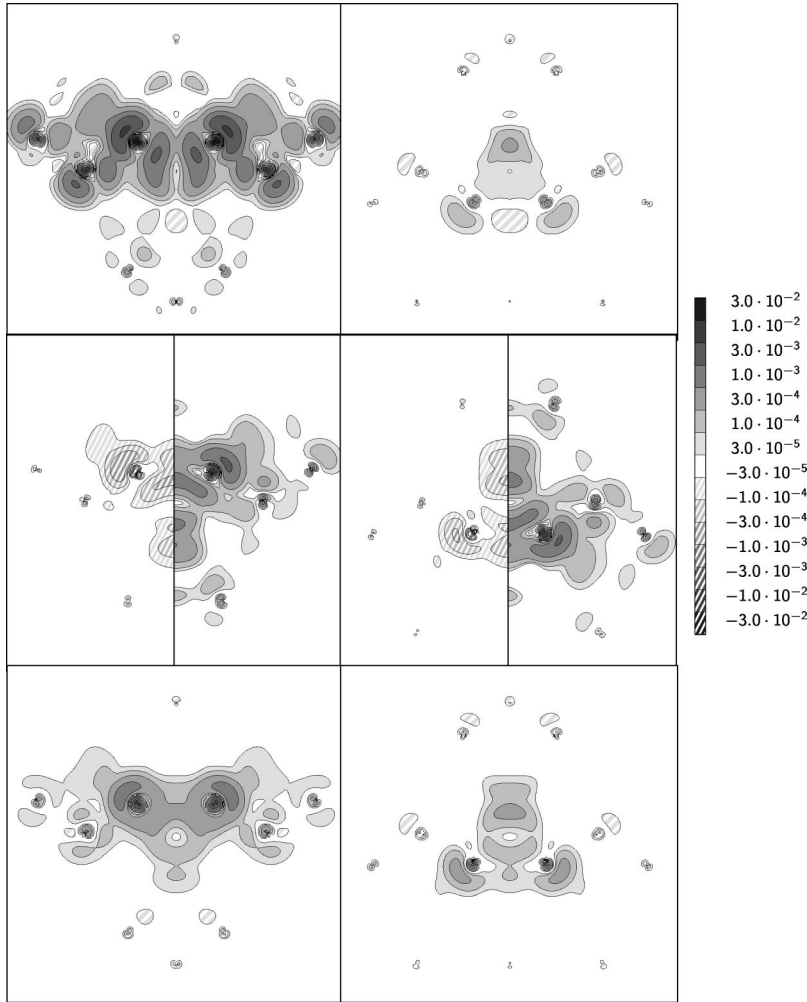


FIG. 4. Contour plots for the  $V^-$  vacancy. The top row shows the total magnetization density in the  $(1\bar{1}0)$  plane (left) and in the  $(110)$  plane (right). In the center row the figures are split into magnetization density (left half) and particle density (right half) for the  $a_1''$  state in the  $(1\bar{1}0)$  plane (left figure) and the  $(110)$  plane (right figure). In the lower row the magnetization density induced in the valence band is shown in the  $(1\bar{1}0)$  plane (left) and in the  $(110)$  plane (right).

would lead to a magnetization density that does not show the prominent  $b_1$ -like symmetry of the group  $C_{2v}$  (see Fig. 4), but would be similar to the *particle density* for the  $a_1''$  gap state with similar HF interactions for comparable nuclei in the  $Mad$  and the  $Mbc$  planes.

It is also interesting to compare the magnetization densities with those expected from a CI calculation that starts from a nonspin-polarized calculation. Figure 5 presents a sketch of the occupied single-particle states of  $V^-$  that transform according to the  ${}^2B_1$  irreducible representation of  $C_{2v}$ . For the ground state  $\Psi_0$  the  $b_1$  state is singly occupied and, therefore, this state has no spin density in the  $(110)$  plane. The same is true for the  $\Psi_1$  and  $\Psi_2$  excited states. In contrast, for the excited states  $\Psi_3$  and  $\Psi_4$  both the  $a_1'$  and  $a_1''$  states are singly occupied. Comparison with Fig. 4 shows that the LSDA calculation predicts the dominant term in the CI calculation to be  $\Psi_4$ : the total magnetization density in the  $(110)$  plane can well be approximated by the particle density of a  $a_1'$  state fractionally occupied as spin-up (represented by the magnetization density induced into the valence band states in the LSDA calculation) and the particle density of a  $a_1''$  gap state fractionally occupied as spin down. The validity of this picture could be checked by the sign of the HF interactions with the  ${}^{29}\text{Si}$  ligands in the  $(110)$  plane. Unfortunately, for the ENDOR data the absolute signs have not

been determined. We thus can only hope that the LSDA treatment, capable to calculate the modulus of the contact interactions with  ${}^{29}\text{Si}$  nuclei in the  $Mbc$  plane, predicts the correct sign as well.

#### IV. CONCLUSIONS

We have calculated the lattice relaxations caused by the lattice vacancy in silicon in the negative charge state using

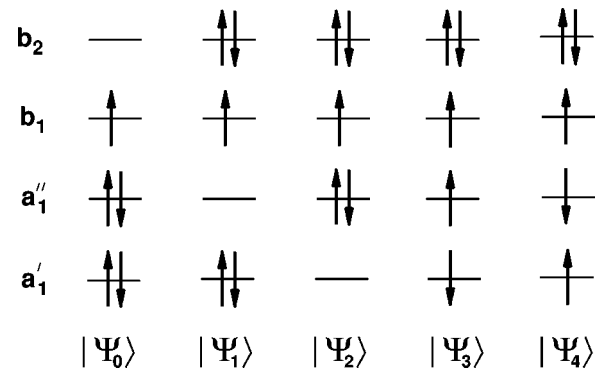


FIG. 5. Schematic representation of the occupation of the single-particle states that give rise to the ground state  $\Psi_0$  of the  $V^-$  and to those excited states of  $V^-$  that transform according to the  ${}^2B_1$  irreducible representation of the group  $C_{2v}$ .

the SCC-DFTB method. On the basis of these relaxed coordinates we have calculated the total energy of high-spin and low-spin configurations of  $V^-$  in the LSDA approximation. We find a low-spin  ${}^2B_1$  ground state with  $C_{2v}$  symmetry as observed experimentally with a total energy that is 0.09 eV below that of the  ${}^4A_2$  high-spin state with  $T_d$  symmetry. This should be contrasted with the negative charge state of the Si vacancy in 3C-SiC and with the vacancy in diamond which both have the tetrahedrally symmetric high-spin  ${}^4A_2$  ground state.<sup>20,21</sup> The reason for this difference is twofold: the dangling bond states in Si are less compact which for the vacancy in Si reduces the energy gain due to spin alignment if compared to the vacancies in SiC and diamond. The larger overlap of the less compact Si dangling bonds leads to strong ( $a-d$ ) and ( $b-c$ ) pairing causing the large Jahn-Teller distortions<sup>18</sup> for the vacancies that give rise to Si dangling bonds.

For the  $V^-$  in the  ${}^2B_1$  low spin state we find that the calculated magnetization density distribution, while still essentially conserving the nodal plane structure of the  $b_1$  gap state, is nonzero at the  $Mbc$  nuclei in the (110) plane. Calculated HF interactions for nuclei in both the (110) and the (110) plane compare well with experimental ENDOR data. In particular the agreement for the nuclei in the (110) plane is surprisingly good in view of the rather indirect nature of the spin polarization in this plane. There is, therefore, no need to infer configuration interactions in order to explain the hyperfine interactions for the lattice vacancy in Si in the  $V^-$  charge state.

#### ACKNOWLEDGMENT

It is a pleasure to acknowledge partial financial support from the Deutsche Forschungsgemeinschaft for this work.

\*Corresponding author. Tel.: + 49-5251-602334, E-mail address: h.overhof@phys.upb.de

<sup>1</sup>G.D. Watkins, in *Radiation Damage in Semiconductors*, edited by P. Baruch (Dunod, Paris, 1965), pp. 97.

<sup>2</sup>G.D. Watkins, in *Deep Centers in Semiconductors*, edited by S. T. Pantelides (Gordon and Breach, New York, 1986), pp. 147.

<sup>3</sup>J. Bernholc, N.O. Lipari, and S.T. Pantelides, *Phys. Rev. Lett.* **41**, 895 (1978); *Phys. Rev. B* **21**, 3545 (1980).

<sup>4</sup>G.A. Baraff, E.O. Kane, and M. Schlüter, *Phys. Rev. B* **21**, 5662 (1980).

<sup>5</sup>G.D. Watkins and J.R. Troxell, *Phys. Rev. Lett.* **44**, 593 (1980).

<sup>6</sup>M. Scheffler, J.P. Vigneron, and G.B. Bachelet, *Phys. Rev. B* **31**, 6541 (1985).

<sup>7</sup>M.J. Puska, S. Pöykkö, M. Pesola, and R.M. Nieminen, *Phys. Rev. B* **58**, 1318 (1998).

<sup>8</sup>J.L. Mercer, J.S. Nelson, A.F. Wright, and E.B. Stechel, *Modell. Simul. Mater. Sci. Eng.* **6**, 1 (1998).

<sup>9</sup>A. Antonelli, E. Kaxiras, and D.J. Chadi, *Phys. Rev. Lett.* **66**, 2088 (1998).

<sup>10</sup>M. Sprenger, S.H. Muller, E.G. Sieverts, and C.A.J. Ammerlaan,

*Phys. Rev. B* **35**, 1566 (1987).

<sup>11</sup>O. Sugino and A. Oshiyama, *Phys. Rev. Lett.* **68**, 1858 (1992).

<sup>12</sup>M. Lannoo, *Phys. Rev. B* **28**, 2403 (1983).

<sup>13</sup>Th. Frauenheim, G. Seifert, M. Elstner, Z. Hajnal, G. Jungnickel, D. Porezag, S. Suhai, and R. Scholz, *Phys. Status Solidi B* **217**, 41 (2000).

<sup>14</sup>H-J. Monkhorst and J.D. Pack, *Phys. Rev. B* **13**, 5188 (1976).

<sup>15</sup>O. Gunnarson, O. Jepsen, and O.K. Anderson, *Phys. Rev. B* **27**, 7144 (1983).

<sup>16</sup>D.M. Ceperley and B.J. Alder, *Phys. Rev. Lett.* **45**, 566 (1980).

<sup>17</sup>P. Perdew and A. Zunger, *Phys. Rev. B* **23**, 5048 (1981).

<sup>18</sup>A. Zywietz, J. Furthmüller, and F. Bechstedt, *Phys. Status Solidi B* **210**, 13 (1998).

<sup>19</sup>A. Zywietz, J. Furthmüller, and F. Bechstedt, *Phys. Rev. B* **59**, 15 166 (1999).

<sup>20</sup>T. Wimbauer, B.K. Meyer, A. Hofstaetter, A. Scharmann, and H. Overhof, *Phys. Rev. B* **56**, 7384 (1997).

<sup>21</sup>J. Isoya, H. Kanda, Y. Uchida, S.C. Lawson, S. Yamasaki, H. Itoh, and Y. Morita, *Phys. Rev. B* **45**, 1436 (1992).

<sup>22</sup>E.O. Kane, *Phys. Rev. B* **31**, 5199 (1985).